ACS Synthetic Biology

pubs.acs.org/synthbio

Research Article

Genome-Scale Metabolic Model Reconstruction and Investigation into the Fluxome of the Fast-Growing Cyanobacterium *Synechococcus* sp. PCC 11901

Somdutt Ravindran,[‖] Nima Hajinajaf,[‖] Pritam Kundu, Jackson Comes, David R. Nielsen, Arul M. Varman,* and Amit Ghosh*

Cite This: *ACS Synth. Biol.* 2024, 13, 3281−3294

Read Online

ACCESS | Metrics & More | Article Recommendations | Supporting Information

ABSTRACT: The ability to convert atmospheric CO_2 and light into biomass and value-added chemicals makes cyanobacteria a promising resource microbial host for biotechnological applications. A newly discovered fastest-growing cyanobacterial strain, *Synechococcus* sp. PCC 11901, has been reported to have the highest biomass accumulation rate, making it a preferred target host for producing renewable fuels, value-added biochemicals, and natural products. System-level knowledge of an organism is imperative to understand the metabolic potential of the strain, which can be attained by developing genome-scale metabolic models (GEMs). We present the first genome-scale metabolic model of *Synechococcus* sp. PCC 11901 (iRS840), which contains 840 genes, 1001 reactions, and 944 metabolites. The model has been optimized and validated under different trophic modes, i.e., autotrophic and mixotrophic, by conducting an *in vivo* growth experiment. The robustness of the metabolic network was evaluated by changing the biomass coefficient of the model, which showed a higher sensitivity toward pigments under the photoautotrophic condition, whereas under the heterotrophic condition, amino acids were found to be more influential. Furthermore, it was discovered that PCC 11901 synthesizes succinyl-CoA via succinic semialdehyde due to its imperfect TCA cycle. Subsequent flux balance analysis (FBA) revealed a quantum yield of 0.16 in silico, which is higher compared to that of PCC 6803. Under mixotrophic conditions (with glycerol and carbon dioxide), the flux through the Calvin cycle increased compared to autotrophic conditions. This model will be useful for gaining insights into the metabolic potential of PCC 11901 and developing effective metabolic engineering strategies for product development.

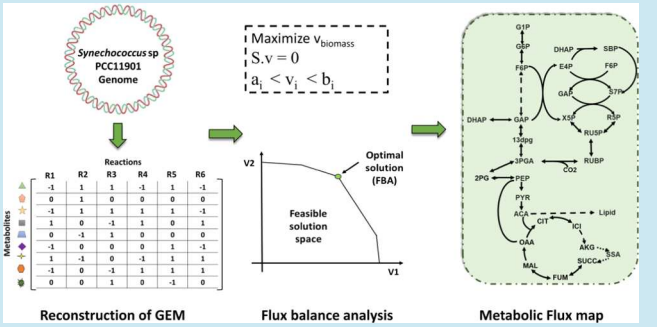

KEYWORDS: *cyanobacteria, metabolic flux analysis, flux variability analysis, dynamic flux balance analysis*

1. INTRODUCTION

Photosynthetic organisms can capture solar energy and convert atmospheric carbon dioxide into valuable compounds.[1] These compounds serve as promising precursors for the synthesis of renewable fuels and value-added chemicals. The current production of petroleum-based chemicals releases greenhouse gases into the atmosphere, such as CO_2, CO, N_2O, and others.[2] Photosynthetic organisms can aid in the sequestration of atmospheric CO_2, a potent greenhouse gas, while synthesizing valuable molecules such as lipids, biopolymers, and pigments. In this regard, plants, microalgae, and cyanobacteria have captured the scientific community's attention as they offer solutions to the global challenges posed by the adverse environmental impact of fossil fuels. Among these organisms, cyanobacteria can be a promising candidate for sustainable biofuel production due to their fast growth rate, remarkable carbon sequestration ability, minimal nutrient requirements, adaptability to different environmental conditions, and relatively easy genetic manipulation.[3]

Over the years, several cyanobacterial strains, i.e., *Synechococcus* sp. PCC 7002,[4] *Synechocystis* sp. PCC 6803,[5] *Synechococcus elongatus* PCC 7942,[6] and *S. elongatus* UTEX 2973[7] have been studied as model organisms for understanding the photosynthetic mechanism and the production of different value-added compounds. The sustainable production of bioplastics,[8] ethanol,[9] free fatty acids,[10] and terpenoids[11] has been reported for these cyanobacterial strains through genetic engineering. For instance, *S. elongatus* PCC 7942 has been

Received: May 28, 2024
Revised: September 5, 2024
Accepted: September 6, 2024
Published: September 19, 2024

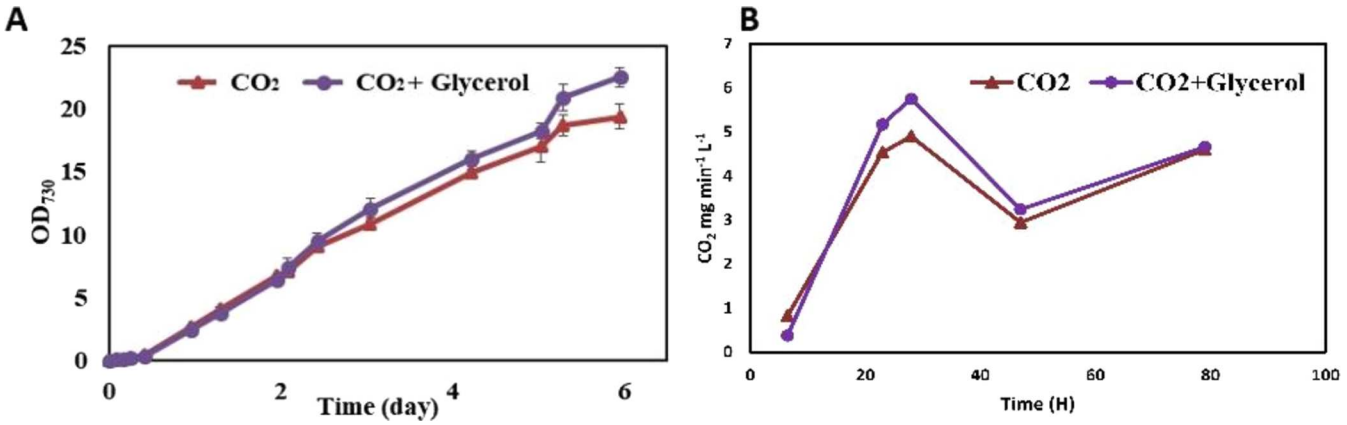

Figure 1. Cultivation of PCC 11901 in the MAD medium. (A) Growth analysis of PCC 11901 under glycerol +1% CO_2 and 1% CO_2 used as controls. (B) CO_2 uptake rate of PCC 11901 with glycerol +1% CO_2 and 1% CO_2.

engineered with genes encoding non-native pyruvate decarboxylase and alcohol dehydrogenase to produce ethanol.[12] Further, the same organism has been used to synthesize 1.1 g L^{-1} of isobutyraldehyde by diverting the carbon flux from the valine biosynthesis pathway with the addition of ketoacid decarboxylase.[13] Other economically important chemicals produced via heterologous biosynthetic pathways in cyanobacteria include 1-butanol,[14] 2,3-butanediol,[15] and ethylene[16] with a titer of 29.9 mg L^{-1}, 2.38 g L^{-1}, and 45.12 mL L^{-1} day^{-1}, respectively. It is evident that cyanobacteria are flexible and can be utilized to develop industrially significant products.[17]

The recently isolated novel cyanobacterial strain *Synechococcus* sp. PCC 11901[10] (PCC 11901 from here) was reported to be the fastest-growing cyanobacterium, with a doubling time of only ≈2 h. In addition, PCC 11901 can grow under high light intensity[18] (900 μmol photons m^{-2} s^{-1}) and salinity (5%), which can lead to a significant dry cell weight (∼33 g/L) that is 2−3 folds higher than the existing model cyanobacterial strains. Furthermore, genetic engineering in PCC 11901 has improved free fatty acid production to 6 mM (1.5 g L^{-1}), which is particularly interesting for industrial applications.[10] These features make the newly isolated cyanobacterium a potential green cell factory for the sustainable biosynthesis of industrially relevant carbon-based molecules through the biosequestration of atmospheric carbon. Nevertheless, in order to identify, evaluate, and develop efficient strain for product development, it is imperative to extensively analyze the system-level information on the organism.

The genome-scale metabolic model (GEM) will serve as a computational framework for exploring and evaluating the metabolic potential of an organism by providing a flux distribution across metabolic pathways. GEM has been considered an effective systems biology tool for understanding the fluxome and simulating the complex metabolic pathways of microbial species. The genome-scale metabolic models of several cyanobacterial strains have been developed over the past few decades, and they have been successfully used for product development. In the following years, the GEMs of *Synechococcus* sp. PCC 7002,[19,20] *Synechocystis* sp. PCC 6803,[5] *S. elongatus* PCC 7942,[21] and *S. elongatus* BDU 130192[22] have been developed by several research groups for biotechnological applications. The metabolic networks of *Synechocystis* sp. PCC 6803 have been well-developed due to the continual improvement of the genome-scale model. The *Synechocystis* sp. PCC 6803 model has been used to support metabolic engineering of the fatty acid pathway gene DGAT, enabling a quantitative insight into flux distribution and further investigation into the effects of glycerol-3-phosphate production on lipid biosynthesis.[23] Furthermore, in PCC 6803, flux balance analysis (FBA) predicted the deletion of the *nadhf1* gene responsible for the reoxidation of NADP(H), which resulted in the enhanced production of ethanol.[9] In another study, using the minimization of metabolic adjustment (MOMA) algorithm, FBA predicted disruption of some of the genes in the NDH-1 complex, resulting in the enhanced titer of 1,3-propanediol and glycerol in *S. elongatus* PCC 7942.[24] Thus, the reconstruction of the genome-scale model and flux analysis strategies will help to effectively understand the system-level behavior of the biochemical pathway of the newly discovered PCC 11901 and assist in rational metabolic engineering.

Here, the first genome-scale metabolic model (iRS840) of the fastest-growing cyanobacterial strain *Synechococcus* sp. PCC 11901 has been reconstructed with available genomic information. The iRS840 was optimized under different trophic modes (autotrophic and mixotrophic), and the in silico growth rate was validated against the *in vivo* experiment. Further, model validation was performed through gene essentiality analysis with the available gene knockout data. In addition, the model was subjected to a biomass sensitivity analysis (SA) to identify the effect of biomass precursors on the model growth rate and metabolic properties. The distinct metabolic behavior and flux distribution in the biochemical network under various growth conditions were also predicted with flux balance analysis (FBA) and flux variability analysis (FVA). Finally, the dynamic FBA (dFBA) was performed utilizing an experimentally derived carbon dioxide uptake rate to simulate batch cultivation of PCC 11901 for biomass production and carbon source(s) utilization patterns. The integration of modeling and experimentation has enabled us to comprehend the intricate metabolic changes of *Synechococcus* sp. PCC 11901 with respect to different trophic modes.

2. RESULTS AND DISCUSSION

2.1. Cultivation of *Synechococcus* sp. PCC 11901 under Different Growth Conditions. PCC 11901 has been shown to have a high growth rate with a doubling time of 2−3 h under optimal conditions.[10] Hence, to investigate this further, growth characteristics studies were conducted under different trophic modes. Initially, PCC 11901 was grown under

https://doi.org/10.1021/acssynbio.4c00379
ACS Synth. Biol. 2024, 13, 3281−3294

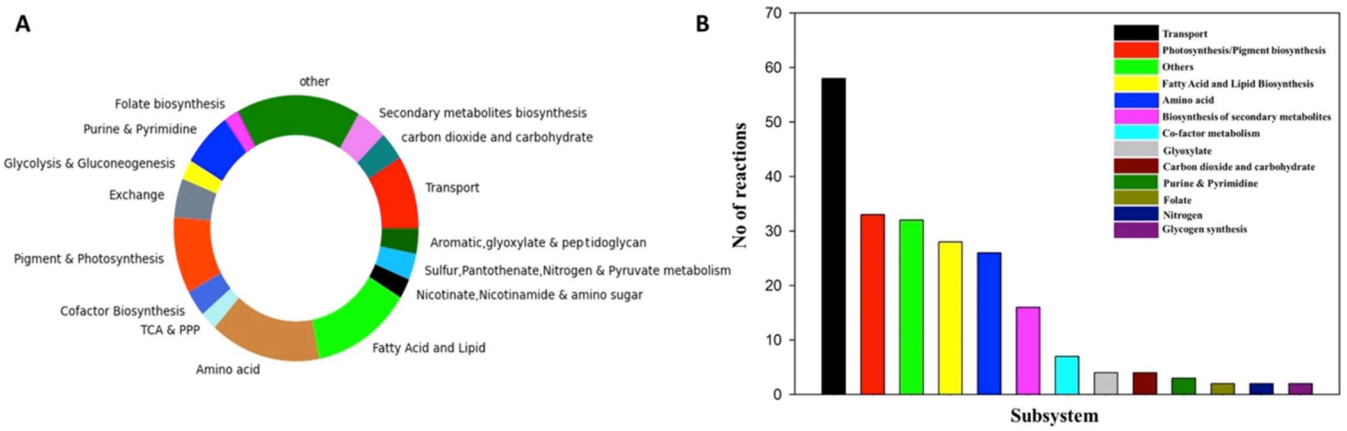

Figure 2. Genome-scale metabolic reconstruction of *Synechococcus* sp. PCC 11901. (A) The pathway level subsystem statistics for reactions. (B) The number of reactions was added to the model by manual gap filling in various compartments.

photoautotrophic conditions, and the growth rate was determined to be 0.063 and 0.151 h^{-1} under atmospheric CO_2 and 1% CO_2 as the carbon source, respectively. Subsequently, the CO_2 uptake rate of PCC 11901 was experimentally calculated when 1% CO_2 was supplied. It was observed that, initially, the CO_2 uptake was high, reaching up to 4.9 mg min^{-1} L^{-1} at 28 h and exhibited almost constant uptake until 78 h; however, the uptake rate decreased, reaching 2.42 mg min^{-1} L^{-1} by day 6 (Figure 1B). The findings align consistently with those of prior research studies.[10] To further evaluate the growth characteristics, PCC 11901 was cultivated under mixotrophic conditions using glycerol, along with 1% CO_2 (Figure 1A). When the PCC11901 was cultured in 1% CO_2 along with glycerol under the mixotrophic condition, it was observed that cells demonstrated a marginally accelerated growth rate, reaching an OD_{730} of up to 22.5. In contrast, under photoautotrophic conditions (1% CO_2), the OD_{730} was 19.4, which is ≈14% less compared to the mixotrophic condition. Further, it was noted that with 1% CO_2, the CO_2 uptake rate of PCC11901 under the mixotrophic condition exhibited a variation of 5.8−2.1 mg min^{-1} L^{-1} in glycerol (Figure 1B). Overall, under mixotrophic conditions, the growth rate and CO_2 uptake were marginally higher compared to the photoautotrophic condition.

2.2. Genome-Scale Metabolic Model Reconstruction and Refinement of *Synechococcus* sp. PCC 11901. The newly discovered fast-growing cyanobacterial strain PCC 11901 can serve as a potential model strain for biotechnological application. Because of the recent discovery of this cyanobacterial strain, knowledge of its biochemical pathways and metabolic features remained mostly unexplored. The genome-scale metabolic modeling strategy will help reveal the system-level biochemical characteristics of this fast-growing cyanobacterial strain in terms of metabolic fluxes. Thus, for the reconstruction of the first genome-scale metabolic model (GEM) of PCC 11901, the whole genome sequence was obtained from the NCBI database under the accession number GCA_005577135.1.[10] The annotated genome sequence was employed in the ModelSEED server[25] to generate a draft GEM of PCC 11901. The initial model contained 18.4% unbound reactions, leading to multiple reaction cycles that neither produce nor consume any metabolites. These reaction cycles lack a thermodynamic driving force, thus making the net flux zero. These thermodynamically infeasible cycles were eliminated by removing the duplicate reactions, turning off the lumped reaction, and selectively turning the reactions on/off based on the available cofactor specificity information from ModelSEED and the literature. Further, it was noted that the model contained multiple orphan metabolites that did not participate in any metabolic pathways and were primarily associated with only one reaction. These metabolites were either removed or connected to the appropriate metabolic pathways. To further enhance the quality of the model, the reversibility of the reactions was checked, and they were corrected by appropriately assigning the directionality by changing the lower and/or upper bounds upon referring to the ModelSEED reaction database and the literature. The model also included 45.14% blocked reactions, which were the result of missing reactions in various metabolic pathways. These reaction gaps were associated with central metabolism, lipids, amino acids, cofactors, photosynthesis, pigment reactions, etc. Further, we have performed the manual gap filling using the KEGG[26] pathway database, ModelSEED reactions databases,[25] PubChem,[27] BiGG Database,[28] and information from the literature.[4,5,19,20,29] The previously published cyanobacterial metabolic models, i.e., PCC6803 (iJN678), *Synechococcus* sp. PCC7002,[19,20] *Synechocystis* sp. PCC 6803[29] and *S. elongatus* BDU 130192[22] were utilized during the curation of the draft model. PCC 11901 is closely related to PCC 7002,[10] and its metabolic pathways remain highly conserved when compared to that of PCC6803.[18] A total of 221 reactions were manually added to the draft model, constituting 22.26% of the total reactions in the reconstructed model, which were majorly involved in photosynthesis and pigment biosynthesis pathways (Figure 2B). These reactions are required to harvest photons and utilize light energy to catalyze the fundamental photosynthetic endergonic processes, which result in high-energy molecules. Furthermore, pigments synthesized by various biochemical pathways are essential for maintaining the metabolic flux through photosynthetic reactions. In the pigment biosynthesis pathway, a vital reaction catalyzed by chlorophyll synthase has been incorporated into the model using available cyanobacterial knowledge.[19] This enables the production of chlorophyll, an important molecule of the pigment biosynthesis pathway. Besides photosynthesis and pigment biosynthesis, several reactions associated with amino acid and folate biosynthesis have been added during the model refinement. It was estimated that ∼11.8% of the total added reaction belonged to amino acid metabolism (Figure 2B). Along with these metabolic reactions, transport and exchange

https://doi.org/10.1021/acssynbio.4c00379
ACS Synth. Biol. 2024, 13, 3281−3294

Table 1. List of GEMs Reconstructed for Cyanobacteria

cyanobacteria	*Synechococcus* sp. PCC 7002[20]	*Synechococcus* sp. BDU 130192 (iSyn706)[22]	*Cyanothece* sp. ATCC 51142 (iCce806)[31]	*Synechocystis* PCC 6803 (iSyn731)[29]	*Arthrospira platensis* NIES-39[32]	*Synechococcus* sp. PCC 11901 (this study)
metabolites	697	900	587	996	673	944
reactions	742	908	719	1156	746	1001
genes	728	706	806	731	644	840

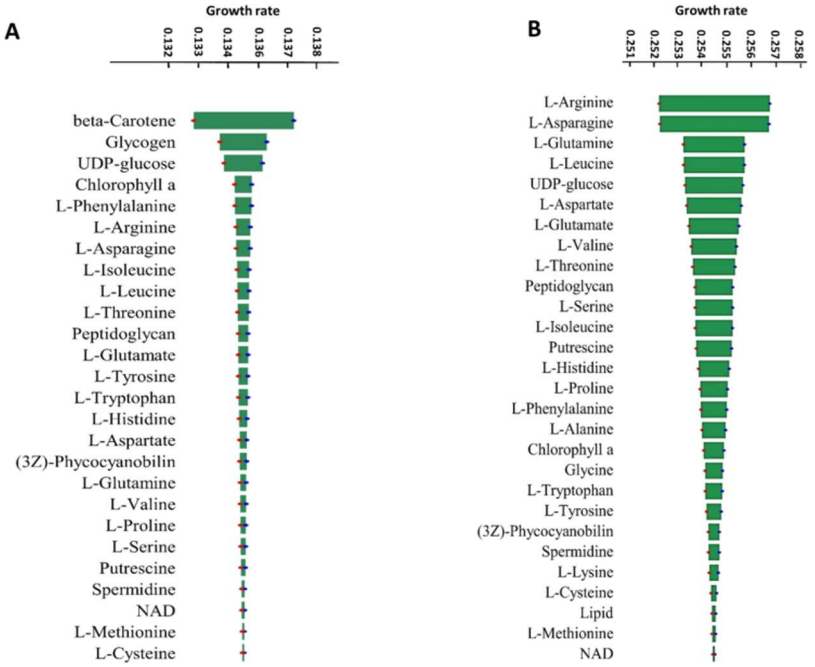

Figure 3. Sensitivity analysis of the biomass objective function in different growth conditions. The effect of a 10% alteration of each biomass precursor on the specific growth rate of PCC 11901 has been represented for (A) autotrophic and (B) heterotrophic conditions. FBA was performed in each step to obtain the specific growth rate during biomass coefficient alteration. Autotrophic and heterotrophic were simulated using CO_2 (4.1 mmol gdw^{-1} h^{-1}) and glycerol (2.2 mmol gdw^{-1} h^{-1}) as carbon sources.

reactions of carbon dioxide, oxygen, glycerol, etc., were added to the model to facilitate the intercompartmental movement of different metabolic compounds. Furthermore, the ATP maintenance requirement in the PCC 11901 model has been denoted by the ATP hydrolysis rate, which was quantified by constraining the model with experimentally measured CO_2 uptake rate and maximizing the flux through the ATP_ase reaction:[30] ATP + H2O → ADP + Pi + H+. For the PCC 11901 model, the ATP maintenance flux was set to be 2.7 based on the recently developed model of *Synechococcus* sp. (iSyn706).[22] Finally, the genome-scale metabolic model of *Synechococcus* sp. PCC 11901 (iRS840) contains 840 genes, 1001 reactions, and 944 metabolites (Tables S1 and S2). There are 79 metabolic transport and 49 exchange reactions available in the model. The model possesses metabolic pathways associated with photosynthesis, pigment production, carbohydrate metabolism, fatty acid biosynthesis, amino acid metabolism, folate metabolism, etc. Apart from the cytosol, two additional compartments, i.e., periplasm and thylakoid, were incorporated into the model, and all of the reactions were localized in these compartments. Further, PCC11901 GEM was compared with other known cyanobacterial models that showed distinct numbers of genes, reactions, and metabolite compositions in each model (Table 1). Moreover, the detailed metabolic profile of PCC 11901 was assessed against those of other published cyanobacterial models to identify the unique metabolites. A total of 260 unique metabolites were observed, which were not found in the other five models (Table S3). The identified metabolites were associated with various metabolic pathways, including amino acid metabolism, ubiquinone and terpenoid-quinone production, and porphyrin, chlorophyll, and pigment biosynthesis, among other things. The metabolic reactions were categorized into various subsystems such as amino acid metabolism, photosynthesis, pigment biosynthesis, folate metabolism, TCA cycle, etc. (Figure 2A). The model was further analyzed to understand the metabolic flux distribution pattern in essential metabolic pathways specific to different growth conditions.

2.2.1. Formulation of Biomass Objective Function for Optimizing iRS840. In the genome-scale metabolic model, the biomass reaction is the compilation of precursor metabolic molecules, like amino acids, carbohydrates, lipids, vitamins, cofactors, and ions, with specific coefficients representing cell biomass production. The biomass precursor constituents and their corresponding coefficients have been adopted from the previously characterized, closely related cyanobacterial species PCC7002.[10] The average nucleotide identity (ANI) and functional identity (AF) between these two strains were 96.5 and 86.4%, respectively. Thus, the biomass equation of the previously published PCC 7002 model was adopted with the necessary modification for formulating the biomass equation of PCC 11901. Based on each autotrophic, mixotrophic, and heterotrophic growth condition, necessary modifications have been made to the biomass composition. The biomass equation

https://doi.org/10.1021/acssynbio.4c00379
ACS Synth. Biol. 2024, 13, 3281−3294

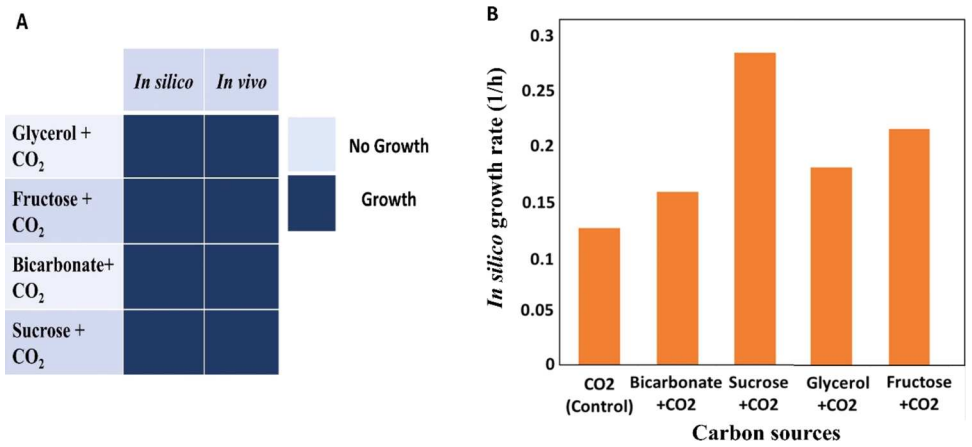

Figure 4. Viability and growth of *Synechococcus* sp. PCC 11901 in various carbon sources under mixotrophic conditions. (A) Comparative analysis of *in silico* and the *in vivo* viability on multiple carbon sources. (B) *In silico* mixotrophic growth rate (1/h) was simulated by the FBA of PCC11901 on different carbon sources.

contained 64 metabolic components. The biomass equation incorporates pigments like β-carotene, chlorophyll a, (3Z)-phycocyanobilin, and β-cryptoxanthin by considering photosynthetic pathways. The *in silico* growth rate under autotrophic and mixotrophic was observed to be ∼0.135 and 0.181 h^{-1}, respectively.

Following the biomass equation formulation, the condition-specific biomass reactions were subjected to sensitivity analysis for further validation. Additionally, the model was utilized to gain insight into and identify metabolites that exhibit sensitivity under various trophic conditions. Here, the effect of coefficient alteration (±10%) of the biomass precursors on the autotrophic, heterotrophic, and mixotrophic growth rates has been checked through FBA. In autotrophic conditions, a 10% fluctuation of the biomass precursor's coefficient altered the biomass formation rate by an average of ∼1.31% (Figure 3A). In heterotrophic and mixotrophic conditions, a 10% alteration in the biomass precursor's coefficient changed the specific growth rate by an average of ∼1.15 and ∼1.05%, respectively. Thus, the minute fluctuation in the specific growth rates signifies the robust metabolic characteristic of the PCC 11901 model under different growth conditions. Further, growth rate variation toward the alteration of each biomass precursor was examined across all growth conditions to identify growth condition-specific sensitive metabolites. The model-specific growth rate was sensitive toward pigments, i.e., β-carotene and β-cryptoxanthin, in the autotrophic and mixotrophic growth conditions, where >1% fluctuation in the model growth rate has been observed. The same positive correlation between pigments and growth was observed in *A. platensis* FACHB-314, wherein applying external chemical stimuli led to the up-regulation of genes (*cobA*/*hemD*, *hemG*, and *ho*) associated with the production of pigment intermediate molecules. Subsequently, this results in increased biomass and enhanced growth due to high pigment accumulation.[33] Apart from the pigments, alteration of the coefficient in the amino acids has a minimal effect (<1%) on the specific growth rate (Figure 3A). In the heterotrophic condition, although the pigments were present in the biomass equation, the specific growth rate was found to be more sensitive to L-arginine (∼1.3%) and L-asparagine (∼1.3%) (Figure 3B). This could be because, in heterotrophic conditions, the amino acid content is higher compared to other growth conditions.[34] Also, in cyanobacteria, certain amino acids, such as arginine, exhibit multifaceted functionality, serving as a building block for protein biosynthesis while concurrently operating as a nitrogen buffer system.[35] This may explain the heightened sensitivity of the model to arginine under heterotrophic conditions. Thus, the overall model demonstrated the versatility to accommodate and alter the flux distribution in response to varying growth conditions while maintaining a stable flux distribution during a slight perturbation of the biomass precursor coefficient. Because of the robust character of the metabolic network, it can readjust the flux distribution pattern through different metabolic reactions and maintain a stable specific growth rate.

2.3. Model Validation. *2.3.1. Comparison of the In Silico and In Vivo Growth Rate.* The growth simulations were performed for the metabolic model under photoautotrophic and mixotrophic conditions by using the FBA approach. The modified AD7 medium[10] containing ammonium as the sole nitrogen has been used to calculate the model growth rate. In the autotrophic condition, the iRS840 showed a biomass formation rate of 0.135 h^{-1} while utilizing carbon dioxide (4.1 mmol gdw^{-1} h^{-1}) along with a nitrogen source and essential metal ions in the presence of light (P680 and P700) (Table S4). The photosynthetic quotient (PQ) was found to be comparable to the PQ range of 1.1 ± 0.4 to PQ = 2.1 ± 0.5 in cyanobacterial species.[36] The in silico autotrophic growth rate was in agreement with the experimental growth rate of 0.149 h^{-1}. In the case of mixotrophy, dark cycle and photosynthetic reactions coexist, increasing the energy production needed to fix both carbon sources, thereby effectively accelerating growth rates. Here, glycerol and CO_2 are simultaneously taken up by the system, increasing the amount of carbon entering the system and consequently increasing biomass production. The model-simulated mixotrophic growth rate of 0.181 h^{-1} has been observed using glycerol (0.3 mmol gdw^{-1} h^{-1}) and CO_2 (3.8 mmol gdw^{-1} h^{-1}) as carbon sources. The simulated growth rate exhibited a close resemblance (80.2%) to the experimental growth rate, which was determined to be 0.151 h^{-1}. Similarly, the model's ability to grow in different organic carbon sources in mixotrophic conditions to mimic *in vivo* growth conditions was also evaluated. During the analysis, the model was updated with an uptake rate of 0.3 mmol gdw^{-1} h^{-1} (Figure 4B) for different carbon sources, including, glycerol,

https://doi.org/10.1021/acssynbio.4c00379
ACS Synth. Biol. 2024, 13, 3281−3294

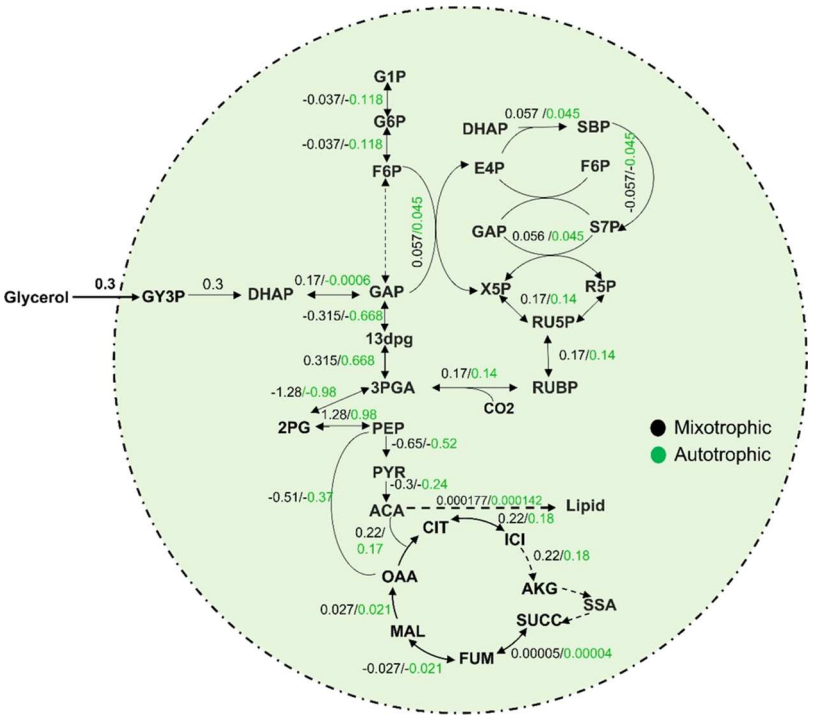

Figure 5. Flux distribution predicted under different growth conditions. The metabolic fluxes of the biochemical reaction in central carbon metabolism in autotrophic (green) and mixotrophic (black) conditions have been represented with a specified color code. In the photoautotrophic conditions, the CO_2 uptake rate was found to be 4.1 mmol gdw^{-1} h^{-1}. In the case of mixotrophic growth, glycerol and the CO_2 uptake rate were fixed at 0.3 and 3.8 mmol gdw^{-1} h^{-1}, respectively.

bicarbonate, sucrose, and fructose, under the mixotrophic condition, which is in agreement with the experimental data (Figure 4A). This indicated that the model possessed all of the intricate metabolic networks required for metabolizing those carbon sources, similar to PCC 11901.

2.3.2. Gene Essentiality Analysis. The gene essentiality analysis has been performed for the model iRS840 to identify the essential genes that are crucial for the cell's viability. Single-gene deletion analysis revealed the presence of 273 critical genes under photoautotrophic conditions. Further, essential and nonessential genes predicted by iRS840 have been compared to the literature gene knockout data. Closely comparable cyanobacterial species *Synechococcus* sp. PCC 7002[10] and *Synechocystis* sp. PCC 6803[18] has been used to validate the gene knockout prediction of iRS840, as the experimental knockout data were unavailable for the newly discovered PCC 11901 strain. *Synechococcus* sp. PCC 11901 showed an average nucleotide identity (ANI) of 96.76 and 73.7%, with PCC 7002[10] and PCC 6803, respectively. The 20 homologous gene knockout data have been available for *Synechococcus* sp. PCC 7002[20] (2 essential and 18 nonessential genes). The model possessed 16 of these 20 homologous genes and correctly predicted 11 nonessential genes. The model mispredicted three nonessential genes associated with amino sugar and nucleotide synthesis, pyruvate metabolism, and carbohydrate metabolism. Further, one essential gene associated with the nitrate reduction reaction was predicted incorrectly (false negative) by the model. The model's specificity was calculated to be 0.785 (GG = 11, NGG = 3), and sensitivity was calculated to be 0.5 (NGNG = 1, GNG = 1) with the available gene knockout data (Table S5). Additionally, the gene essentiality analysis has been conducted using the essential and nonessential genes of *Synechocystis* sp. PCC 6803.[29] The model was able to predict 5 essential genes out of 11, and they were mostly associated with the pigment biosynthesis pathway and transport reaction. In contrast, the model could predict 50 out of 53 nonessential genes used in the model analysis (Table S5). The nonessential genes that were predicted to be essential by the model belong to the reactions associated with photosynthesis, the pigment biosynthesis pathway, and carbohydrate metabolism. According to this analysis, the model's specificity is 0.94 (GG = 50, NGG = 3), and its sensitivity is 0.45 (NGNG = 5, GNG = 6). The occurrence of a few false positives can be ascribed to the potential presence of duplicate genes. Furthermore, even though these cyanobacteria are closely related, their metabolic profiles may differ, which could account for the observed variations in the knockout data. Hence, we have performed FROG (Tables S6–S8) analysis to validate the single-gene deletion predictions obtained from the gene essentiality analysis. The knockout profiles obtained through the FROG analysis (Table S9) showed a good correlation with the earlier gene essentiality analysis under photoautotrophic conditions.

2.4. Comparative Analysis of the *In Silico* Flux Distribution of PCC 11901 under Different Growth Conditions. The *Synechococcus* sp. PCC 11901 strain is metabolically versatile and can utilize different carbon sources to maintain biomass production. How the alteration of the carbon sources under different growth conditions affects the metabolic flux distribution of different biochemical pathways has not been explored. Here, we have checked the metabolic flux distribution of the model for autotrophic and mixotrophic growth with condition-specific constraints (Figure 5). In the autotrophic conditions, the cell transported carbon dioxide from the extracellular environment (4.1 mmol gdw^{-1} h^{-1}), participating in the carbon fixation Calvin cycle. CO_2 is fixed

https://doi.org/10.1021/acssynbio.4c00379
ACS Synth. Biol. 2024, 13, 3281−3294

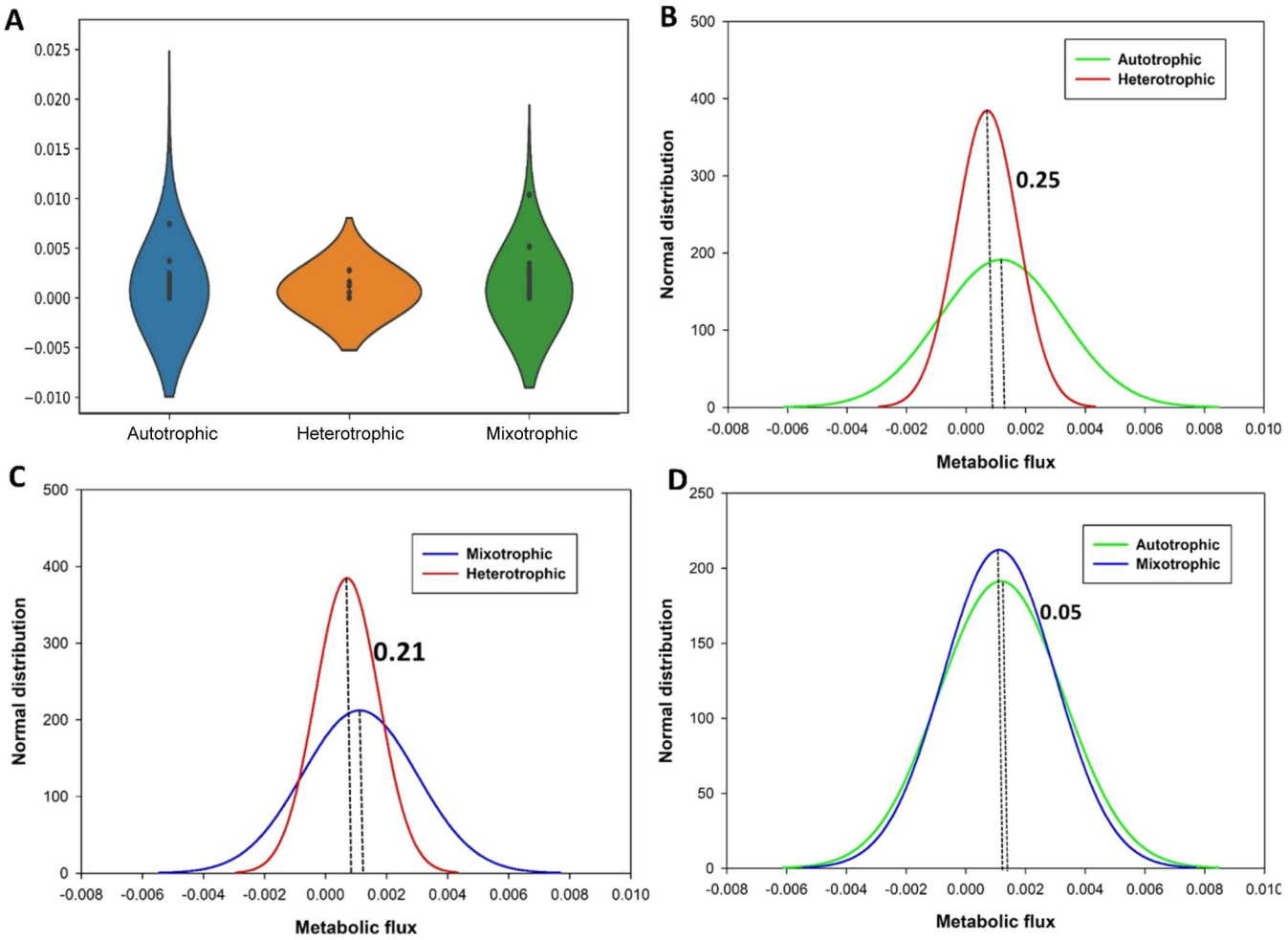

Figure 6. Flux variability analysis of PCC 11901: (A) flux space distribution under three different growth conditions, calculated Cohen's *d* value for normal distribution for the overall flux range under the three trophic modes, (B) autotrophic-heterotrophic (AH), (C) mixotrophic-heterotrophic (MH), and (D) autotrophic-mixotrophic (AM).

by RuBisCO, fueled by the ATP and NADPH generated during photosynthesis, and through 3-PG, the carbon enters the metabolic pathway. Further, in the photoautotrophic conditions, the quantum yield (i.e., CO_2 fixed per photon consumed) was calculated as 0.16 for the PCC 11901 model (Table S10), which was higher than the quantum yield of *Synechocystis* sp. PCC 6803,[37] which was calculated to be 0.072. This finding suggests that PCC 11901 may efficiently utilize a marginally higher concentration of CO_2, while it needs a slightly lower amount of photon input. In addition to other notable attributes, it was observed that alanine demonstrated the highest flux among all amino acids under phototrophic conditions, while valine, tyrosine, tryptophan, threonine, serine, proline, phenylalanine, methionine, lysine, histidine, and leucine exhibited the lowest production flux. The exhibited low amino acid flux pattern aligned with findings reported in other cyanobacterial studies.[38]

In the mixotrophic mode, the organic carbon source glycerol was initially metabolized through the reaction glycerol to glycerol-3-phosphate (glycerol kinase) before entering the central carbon metabolism pathway. This metabolic pathway ultimately gives rise to dihydroxyacetone phosphate (DHAP), which is an essential precursor for the synthesis of S7P (sedoheptulose-7-phosphatase) and RuBP (ribulose-1,5-bisphosphate). This S7P molecule also functions as a rheostat for carbon flux at the interface of glycolysis and the pentose phosphate pathway.[39] These bifunctional enzymes present in the pentose phosphate pathway could assist in the conversion of carbon dioxide into storable carbohydrates within the intracellular matrix, and a comparable mechanism was also proposed within the framework of PCC 7002.[19] In both growth conditions, CO_2 served as the primary carbon source, which may have contributed to the higher 3PGA and 2PG fluxes. Further, it was seen that similar to certain other cyanobacterial strains,[40] PCC 11901 also exhibits an incomplete TCA cycle due to its 2-oxoglutarate dehydrogenase enzyme deficiency. This precludes the direct production of succinate and necessitates the conversion of succinyl semialdehyde into succinate, facilitated by succinate semialdehyde oxidoreductase. Furthermore, the TCA cycle plays a crucial role in providing essential amino acid precursors, as well as carbon skeletons, for nitrogen fixation, specifically in the form of 2-oxoglutarate, and a similar trend was observed in the case of PCC 7002[19] and PCC 6803.[37] Under mixotrophic conditions, the organic carbon source was metabolized through the nonoxidative pentose phosphate pathway to produce ribulose-1, 5-biphosphate, and a substantial flux across RuBisCO was seen to fix the CO_2 that the metabolic network's decarboxylation processes released. The RuBisCO facilitated the necessary flow of 3-phosphoglycerate flux, which was

https://doi.org/10.1021/acssynbio.4c00379
ACS Synth. Biol. 2024, 13, 3281−3294

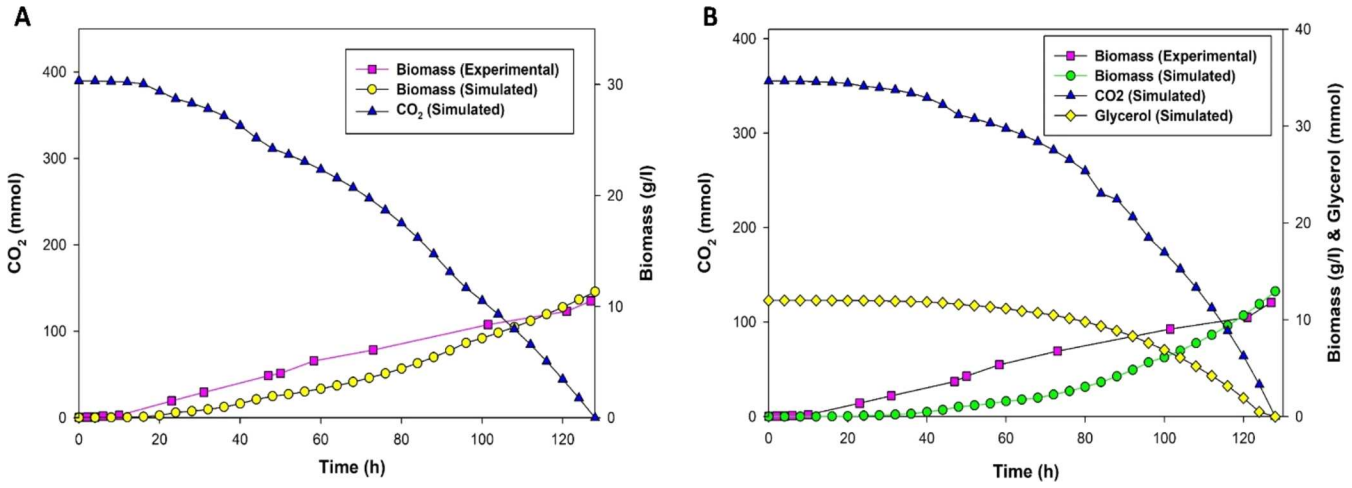

Figure 7. Dynamic flux balance analysis under (A) autotrophic mode and (B) mixotrophic mode.

further separated and channeled toward the TCA cycle, led by the phosphoglycerate mutase (PGM) and subsequently followed by the phosphoglycerate kinase (PGK). Further, under the mixotrophic conditions, there was a significant increase in flux across RuBisCO compared to the autotrophic condition. A comparable pattern was observed in PCC 7002 when it was subjected to an organic carbon source (glycerol), resulting in a 1.5-fold increase in transcription levels of RubisCO.[41] Moreover, the overall H^+/ATP *in silico* flux ratio remained nearly consistent within the range of 4−4.67 observed in *Synechocystis* species.[42−44] Overall, it was noted that the 3PGA and 2PG formation exhibited relatively higher flux under the mixotrophic condition. Also, it was found that substantial pyruvate flux was directed toward acetyl-CoA, i.e., the TCA cycle under the mixotrophic condition compared to other growth conditions. In all growth conditions, the TCA cycle exhibited considerable activity and facilitated the flow of metabolites through the γ-aminobutyric acid (GABA) shunt.

2.5. Flux Variability Analysis of *Synechococcus* sp. PCC 11901 under Different Growth Conditions. Flux variability analysis (FVA) allows us to determine the range of feasible reaction fluxes that satisfy the original FBA constraints within an optimal solution. Additionally, FVA provides valuable information about the flexibility and robustness of the metabolic network. The flux variability range of the PCC 11901 metabolic network was explored in three growth conditions by keeping the optimal biomass production rate at 90%, and the condition-specific flux range of the reactions was determined (Table S11). It was observed that the flux space in autotrophic and mixotrophic conditions expanded compared to that under heterotrophic conditions (Figure 6A). Further, Cohen's *d* effect size was calculated to assess the changes in the flux spaces across the three trophic modes. The effect size (d_s) of the pairwise combination of the three different trophic modes was calculated, and it was found to be 0.05, 0.21, and 0.25 for autotrophic-mixotrophic (AM) (Figure 6D), mixotrophic-heterotrophic (MH) (Figure 6C), and heterotrophic-autotrophic (AH) (Figure 6B), respectively. The effect size indicates a considerable expansion in the flux span under mixotrophy and autotrophy compared with the heterotrophic growth condition. This expansion can be primarily attributed to the reactions associated with pigment and photosynthesis. Further, these pathways were assessed to calculate the pairwise effect size, and it was found to be 0.33, 0.72, and 0.43 for AM, MH, and AH, respectively. The flux space of reactions associated with photosynthesis was observed to be greater under autotrophic and mixotrophic conditions than under heterotrophic conditions. It has been seen that under the mixotrophic conditions, the photochemical efficiency is relatively increased compared to the autotrophic condition. Nevertheless, the autotrophic condition exhibited a better photochemical efficiency compared with the heterotrophic condition. Furthermore, while comparing the total effect size between different growth conditions, it was found that A-H also displayed a considerable effect size (Tables S12−S14). Overall, Cohen's *d* analysis suggests that the photosystems are highly active, and their flux space can be expanded in autotrophic and mixotrophic conditions compared to heterotrophy, and the same was seen in the PCC6803 expression analysis.[45]

In this study, FVA analysis simulated the range of possible metabolic flux for the given reaction(s) within the defined model constraints. It was observed that the heterotrophic mode had a rigid flux space control, indicating that this growth condition may limit the metabolic capacity of the cyanobacteria, which is improved while maintaining the mixotrophic condition. Under the mixotrophic condition, cyanobacterial metabolism becomes more robust, especially in terms of growth rate, and this has been seen in other cyanobacteria like PCC 7942[46] as well. The principal rationale for this is that the synergistic effect that occurs between organic carbon metabolism and photosynthesis under mixotrophic conditions results in increased cellular activity and growth. Further, FVA analysis may help in predicting the optimal growth condition, metabolic pathway constraints, and carbon-feeding strategies for increasing the productivity of biomass and essential biomolecules. Additionally, it can offer essential insights for further genetic engineering to improve the strain's potential.

2.6. Dynamic Flux Balance Analysis for Simulating Biomass Production under Different Growth Conditions. Dynamic flux balance analysis (dFBA) was implemented to establish a match between the simulated and experimental substrate consumption and biomass formation profiles. In order to simulate the time-dependent growth profile of PCC 11901, we used experimentally determined carbon dioxide uptake rates under different time periods (growth phases). In the autotrophic growth conditions, the model was grown under an experimentally calculated average

https://doi.org/10.1021/acssynbio.4c00379
ACS Synth. Biol. 2024, 13, 3281−3294

CO_2 uptake rate, and dFBA was implemented, through which dynamic biomass production and CO_2 consumption data were obtained. Following this, the biomass and CO_2 data acquired from the simulation of the previous growth phase were updated into the model along with the second uptake rate. This updated model was utilized to simulate the subsequent phase. This iterative process was continued until the last phase was simulated. It was observed that the simulated biomass production data were in accordance with the empirical value of *in vivo* biomass. During the simulation, it was observed that there was a brief lag phase of approximately 20 h, following which it entered the exponential phase. Overall, the *in silico* biomass profile concurred with the experimental findings. Further, it was noted that, by 128 h, the simulated biomass concentration had reached up to 11.3 g L^{-1} and was slightly exceeding the *in vivo* total biomass of 10.5 g L^{-1} at 127 h (Figure 7A) (Table S15).

Furthermore, dFBA was executed for mixotrophic conditions, wherein glycerol and CO_2 were utilized as carbon sources. Similar to the autotrophic conditions, simulations were performed for the mixotrophic growth conditions, wherein the sole difference was the utilization of mixotrophic-specific CO_2 and glycerol uptake rates. The model was assigned a glycerol uptake rate of 0.0275 mmol gdw^{-1} h^{-1} with an initial glycerol concentration of 1.12 g L^{-1} (12 mmol). Following the phase-dependent model simulation, it was observed that, overall, the *in silico* biomass exhibited a close resemblance to the experimental values, with minor deviations during the initial exponential phase, which continued up to 96 h. Further, it was observed that the *in silico* scenario demonstrated an overall consistent glycerol consumption pattern, with complete depletion occurring at 124 h, consequently compelling the system to rely solely on CO_2 as the principal carbon source (Table S16). Furthermore, it was noted that until 96 h, there was a consistent decline in overall CO_2; this might be attributed to the comparatively low glycerol consumption seen until 96 h, suggesting a greater dependence on CO_2 within the system. Additionally, it was observed that the simulated CO_2 consumption was more rapid after 96 h. Nevertheless, post-96 h, it was noted that the glycerol consumption was more accelerated, resulting in the system utilizing both carbon sources more evenly. Overall, during in silico analysis, the biomass concentration peaked at 12.93 g L^{-1} at the 128th hour, slightly elevated compared to the *in vivo* value of 11.78 g L^{-1}. Notably, the maximal biomass concentration exhibited a good concurrence with the empirical value, indicating the model's ability to replicate the organism's growth by providing experimentally obtained carbon dioxide consumption uptake rates.

The findings from dFBA indicate that the model successfully replicated the organism's growth and carbon consumption profiles in both autotrophic and mixotrophic conditions. In autotrophic conditions, the model exhibited a greater degree of biomass production profile resemblance to the *in vivo* data. This might be attributed to the utilization of time-dependent CO_2 uptake rates. Further, under the mixotrophic condition, it was observed that the in silico biomass profile was similar to the *in vivo* biomass profile, with only a slight difference in the initial exponential biomass profile. Nevertheless, the mixotrophic material demonstrated a significant increase in biomass production both in silico and *in vivo*, reaching up to 12.93 and 11.78 g L^{-1}, respectively (Figure 7B). The dFBA analysis also showed that under mixotrophy conditions the biomass was enhanced by up to 12.6% compared to autotrophy. The findings indicate that the model successfully replicates the growth pattern of PCC 11901 under both autotrophic and mixotrophic conditions. We have obtained a Pearson correlation coefficient (R) of 0.925 between experimental and simulation dFBA biomass values. Further, the P-value is < 0.00012 (at a significance level of $p < 0.01$) for both autotrophic and mixotrophic growth conditions (Figure S1). Overall, it was observed that the mixotrophic conditions show a significant increase in biomass production, and it can be regarded as a favorable condition. The same trend has been seen in other cyanobacteria as well,[45−47] and this growth condition can be used to achieve a higher cyanobacterial yield.

3. CONCLUSIONS

Our study presents the first genome-scale metabolic network reconstruction of a fast-growing cyanobacterial strain, *Synechococcus* sp. PCC 11901 under different trophic modes. Because of recent discoveries, knowledge of biochemical pathways and metabolic activities is limited. Therefore, reconstruction and analysis of the genome-scale metabolic model of PCC 11901 offer a holistic perspective on metabolic flux distribution, enriching our comprehension of metabolic activities and underlying pathways. The metabolic model has been optimized under different trophic conditions using the experimentally measured CO_2 uptake rate. The specific growth rates predicted by the model were in good agreement with those obtained experimentally. The PCC 11901 showed enhanced capacity and metabolic efficiency under mixotrophic conditions. This is due to the synergistic interaction between organic carbon metabolism and photosynthesis, which boosts cellular activity and growth rates. The dFBA analysis also showed that mixotrophy favored enhanced biomass accumulation, resulting in a 12.6% increase compared with other trophic modes. Further, the flux variability analysis (FVA) predicted optimal growth conditions, identified metabolic constraints, and optimized carbon-feeding strategies to boost biomass productivity and biomolecule synthesis. Hence, the reconstructed GEM will be useful for gaining insights into PCC 11901's metabolic potential and developing effective metabolic engineering strategies for value-added product development.

4. METHODOLOGY

4.1. Chemicals, Culture Medium, and Growth Conditions. A single colony of *Synechococcus* sp. PCC 11901 was picked and streaked on a solid MAD medium plate. The selected colony was cultured in a 150 mL culture flask. Genomic DNA was extracted, and primers (Table S17) were designed to amplify the FEK30_RS01775 gene. The amplified gene was then sequenced to confirm the strain's identity (Table S17). For the growth experiments, PCC 11901 was initially cultured on solid MAD plates for 48 h and then recultured in 100 mL bubble flasks with aeration using atmospheric air for 24 h. For anaerobic and aerobic (air) cultures, cells were taken at the early log phase and recultured in 50 mL Erlenmeyer flasks with a working volume of 10 mL. Cultures were provided with various carbon sources, such as sucrose, fructose, arabinose, glycerol, and bicarbonate. Mixotrophic experiments using 1% CO_2 were accomplished in bubble cultures. To perform higher concentrations of CO_2, cells were transferred to 1% CO_2 chamber for adaptation, and

https://doi.org/10.1021/acssynbio.4c00379
ACS Synth. Biol. 2024, 13, 3281−3294

after 6 h, cells were cultured in 50 mL fresh modified AD7 medium (Table S18). All experiments were performed in triplicate, and an initial optical density (OD) of 0.05 was used. While using shake flasks, cultures were agitated at 250 rpm and grown in ambient air under the light intensity of 200 μmol photons m^{-1} s^{-2}. For cultures under 1% CO_2, cells were initially exposed to 150 μmol photons m^{-1} $s^{-2,}$ and then the light intensity increased to 650 μmol photons m^{-1} s^{-2} after 24 h. Different sugars such as bicarbonate (cas no: 144−55−8, www.sigma.com), fructose (cas no: 57−48−7), glycerol (cas no: 56−81−5), sucrose (cas no: 57−50−1) were also used in this study. Further, the biomass was estimated using the OD value. The conversion factor used was 0.563 (Figure S2).

4.2. CO_2 Uptake Measurement. The culture tubes were equipped with carbon dioxide sensors to measure the composition of the inlet and exhaust gas. In the inlet, pure CO_2 gas was provided from a cylinder and mixed with air using two mass flow controllers (Alicat Scientific, Inc.) and injected into the cultures at a rate of 70 mL/min using a multichannel rotameter (Aalborg). The concentration of inlet and outlet gas was measured using a CO_2 sensor (Vaisala, Finland), and inlet CO_2 concentration was set at 1% CO_2.

To calculate the mass of CO_2 at exhaust (in mg/min/L), the ideal gas law formula was used

$$PV = \left(\frac{m_{CO_2}}{M_{CO_2}}RT\right) \tag{1}$$

where P is the pressure of the environment (Pa), V is the culture volume (mL), R is the ideal gas constant ($m^3 \cdot Pa \cdot K^{-1} \cdot mol^{-1}$), T is the temperature (K), m_{CO_2} is the mass of gas (g), and M_{CO_2} is the molar mass (g mol^{-1}).

To calculate the CO_2 uptake rate, the following formula was used

$$CO_{2_{uptake}} = Q_{gas} \cdot (y_{CO_2,inlet} - y_{CO_2,outlet}) \cdot m_{CO_2} \tag{2}$$

The measured CO_2 uptake rate is in milligrams per minute per liter (mg/min/L) and needs to be converted to millimoles per gram of dry weight per hour (mmol/gdw/h) in order to be utilized as an input flux in the model. The calculations are shown in Table S19.

4.3. Reconstruction of the Genome-Scale Metabolic Model for *Synechococcus* sp. PCC 11901. ModelSEED[25] workspace was used for annotation and generation of draft metabolic model PCC 11901. COBRApy[48] was used in Spyder, Anaconda (Python 3.6) for reading and manipulating the draft model in Systems Biology Markup Language (SBML) format. COBRA Toolbox v3.0[49] was used in MATLAB R2016b. Metabolite formula and charge were added using PubChem,[27] CHEBI (Chemical Entities of Biological Interest),[50] ModelSEED,[25] and BiGG[28] database. Additional reactions were manually added as necessary to produce known biomass constituents or utilize known nutrients through a detailed literature survey; MetaCyc,[51] KEGG,[26] and ModelSEED[25] were used to correct the *Synechococcus* sp. PCC 11901 genome-scale model.

4.3.1. Biomass Sensitivity Analysis in Different Growth Conditions. Sensitivity analysis (SA) is a computational technique used to examine the possible relationships between the input sources and output uncertainty of a particular mathematical model's output.[52] Typically, the results of an SA run are a sorted list of the sensitivity coefficients related to the aforementioned inputs.[53] The objective function of an FBA model is examined in different growth scenarios to see how the growth rate changes in response to a change in the individual components of the biomass by 10%. The sensitivity λ_i^Z represents the response of the objective function Z to a perturbation on the availability of a metabolite i.

$$\lambda_i^Z = -\frac{\partial Z}{\partial b_i^r} \tag{3}$$

where b_i corresponds to the mass balance for metabolite i and superscript r denotes a relaxation in the steady state. It can be noted that if the response of Z to an increment in b_i^r is an increase in its value, then λ_i^Z should be less than zero. On the other hand, if Z decreases λ_i^Z should be greater than zero, and if Z does not change λ_i^Z is equal to zero. In this sense, the sensitivity value can be interpreted as a state of resource availability showing if a given metabolite is limiting ($\lambda_i^Z < 0$), in excess ($\lambda_i^Z > 0$) or has no effect on Z ($\lambda_i^Z = 0$).

4.3.2. Gene Essentiality Analysis. The model was subjected to single-gene deletion analysis to identify essential and nonessential genes. The genes were classified as essential and nonessential based on whether the deletion resulted in a nonviable or viable network,[54−56] respectively. Further, the model-predicted essential and nonessential genes were compared with available gene data from the closely related PCC 6803 and PCC 7002 cyanobacterial stains to calculate the sensitivity and specificity of the model using the following equation[29]

$$\text{specificity} = \frac{\text{GG}}{\text{GG} + \text{NGG}} \tag{4}$$

$$\text{sensitivity} = \frac{\text{NGNG}}{\text{NGNG} + \text{GNG}} \tag{5}$$

where GG is the number of cases where there was both *in silico* and *in vivo* growth. NGG is the number of cases where there was no growth in silico, but there was *in vivo* growth. NGNG is the number of cases where there was no growth *in silico* and *in vivo*. GNG is the number of cases where there was in silico growth but no growth *in vivo*.

4.3.3. Genome-Scale Flux Balance Analysis of Synechococcus sp. PCC 11901 Metabolic Model. The flux solutions under steady-state conditions were ascertained using FBA. All simulations were run in MATLAB with FBA[57] using the COBRA toolbox.[49] The spectrum of potential flow distributions can be characterized by a single optimal solution made achievable via FBA. The linear programming problems were solved using glpk solver. To find the best solution for the metabolic model in our investigation, the biomass equation was maximized. Flux balance analysis was employed in both the validation and testing phases. PCC 11901 models were evaluated in terms of biomass production in different trophic modes: autotrophic, mixotrophic, and heterotrophic. Flux distributions for each one of these states were inferred by using FBA.

Maximize $v_{biomass}$

Subject to

$$\sum_{j=1}^{m} S_{ij} v_j = 0 \quad \forall\, i \in 1, \ldots, n \tag{6}$$

$$V_{j,min} \le V_j \le V_{j,max} \quad \forall\, j \in 1, \ldots, m \tag{7}$$

https://doi.org/10.1021/acssynbio.4c00379
ACS Synth. Biol. 2024, 13, 3281−3294

Here, S_{ij} is the stoichiometric coefficient of metabolite i in reaction j and v_j is the flux value of reaction j. Parameters $V_{j\min}$ and $V_{j\max}$ denote the minimum and maximum allowable fluxes for reaction j, respectively.

The model included three biomass equations: bio1, bio2, and bio3, representing autotrophic, heterotrophic, and mixotrophic conditions, respectively (Table S20). The model's biomass objective functions must be set accordingly to simulate different growth conditions. Further, model's photosynthesis quotient (PQ) was determined, wherein using ratios of oxygen production to carbon dioxide consumption, typical PQ ranges of 1.0−1.8 are reported for algae and photosynthetic marine organisms.[58] Quantum yield is defined as per mole CO_2 fixed per moles of photon consumed,[37] and it was calculated using the following formula

$$\text{quantum yield} = \frac{CO_2 \text{ consumed}}{\text{total photon consumed}} \tag{8}$$

4.3.4. Genome-Scale Flux Variability Analysis of Synechococcus sp. PCC 11901 Metabolic Model. The COBRA toolbox was used to calculate metabolic model fluxes by maximizing the biomass equation. For FVA,[59] the flux variability function was performed. We intended to compare the behavior of a cyanobacterial system under various growth conditions, as the system seeks to attempt to maintain its maximal objective value. This implies that despite growth circumstances, the system always retains the maximum amount of biomass. Therefore, the diversity of each reaction's flux in such a scenario can mirror the flux's narrowness in diverse circumstances. The FVA output consisted of two vectors containing the minimum and maximum fluxes for each reaction. Therefore, the flux range for each reaction could be computed by using the corresponding lowest and maximum values. Additionally, we conducted Cohen's[60,61] (d_s) effect size measurement to assess the variation in flux space pattern in the model as the trophic modes of cyanobacterial cultivation were altered. Equation 9 is utilized to calculate Cohen's effect size

$$(d_s),\ \text{effect size}\ (d_s) = \frac{M_a - M_b}{\text{Sd}} \tag{9}$$

The average flux space values associated with two distinct trophic modes are denoted by M_a and M_b. The aggregated standard deviation of all flux values for the given combination of trophic modes is denoted by Sd. Cohen's (d_s) effect size was determined between mixotrophy-autotrophy, autotrophy-heterotrophy, and mixotrophy-heterotrophy.

4.3.5. Dynamic Flux Balance Analysis Simulations. The reconstructed model underwent dynamic flux balance analysis[62] (dFBA) to computationally simulate batch growth of PCC 11901 under both autotrophic and mixotrophic growth conditions. The computational model simulations were executed utilizing the COBRA Toolbox v3.0.[49] The model inputs were derived from batch cultivations, wherein the maximum uptake rate, initial substrate concentration, and biomass concentration were determined. Subsequently, the utilization of flux balance analysis (FBA) was executed within the aforementioned constraints to determine the fluxes at their maximal growth rate

$$X_{(t+\Delta t)} = X_t \cdot e^{\mu \Delta t} \tag{10}$$

$$S_{(t+\Delta t)} = S_t - V_{EX\_S} \cdot X_t \cdot (1 - e^{\mu \Delta t})/\mu \tag{11}$$

$$P_{(t+\Delta t)} = P_t - V_{EX\_P} \cdot X_t \cdot (1 - e^{\mu \Delta t})/\mu \tag{12}$$

The variables X_t, S_t, and P_t represent the concentrations of biomass, substrate, and product, respectively, at any given time point "t" throughout the cyanobacterial growth. The specific growth rate of the cyanobacterial in h^{-1} is denoted by "μ". The uptake and production rates for the substrate and desired product are denoted as V_{EX_S} and V_{EX_P}, respectively. The time difference between any two time points is denoted as "Δt".

The model was simulated with different growth-phase-specific average CO_2 uptake rates under autotrophic and mixotrophic conditions. The CO_2 uptake rate was measured experimentally in three different phases, i.e., phase I (0−24 h), phase II (24−48 h), and phase III (48−96 h) and phase IV (96−128 h). The average maximum CO_2 uptake rates under autotrophic conditions in phase I, phase II, and phase III and phase IV were 6.1, 2, 1.6, and 0.5 mmol/gdw/h respectively. In the mixotrophic condition, the average uptake rates used in different phases I, II, III, and IV are 5.2, 2.4, 1.2, and 0.6 mmol/gdw/h, respectively. The experimental CO_2 uptake value was not available for each time point; therefore, dFBA has been performed under four distinct average uptake rates to simulate various growth stages of the model.

■ ASSOCIATED CONTENT

Data Availability Statement

The authors declare that all other relevant data are available within the article and its Supplementary Data Files. The metabolic model is available in github (https://github.com/itsamit/Synechococcus-PCC11901).

Supporting Information

The Supporting Information is available free of charge at https://pubs.acs.org/doi/10.1021/acssynbio.4c00379.

Correlation analysis between the experimental and simulation dFBA biomass values under mixotrophic and autotrophic growth conditions (Figure S1) and OD vs dry cell weight (DCW) curve for calculating the biomass conversion factor (Figure S2) (PDF)

List of metabolites present in the model (Table S1); list of reactions present in the model (Table S2); list of GEMs reconstructed for cyanobacteria and other models (Table S3); FBA of the model under different growth conditions (Table S4); essential and nonessential gene comparison with closely related organisms (Table S5); FROG analysis (FVA) (Table S6); FROG analysis (reaction deletion) (Table S7); FROG analysis (optimization) (Table S8); FROG analysis (gene deletion) (Table S9); calculation of *in silico* quantum yield (Table S10); list of overall active and inactive reactions with flux ranges under different growth conditions (Table S11); Cohen's *d* analysis of the mixotrophic and heterotrophic (MH) (Table S12); Cohen's *d* analysis of the mixotrophic and autotrophic (MA) (Table S13); Cohen's *d* analysis of the heterotrophic and autotrophic (AH) (Table S14); dynamic flux balance analysis of autotrophic condition (Table S15); dynamic flux balance analysis of the mixotrophic condition (Table S16); sequencing of FEK30_RS01775 gene (Table S17); AD7 media composition (Table S18); CO_2 uptake rate calculations (Table S19); and list of conditions maintained under different trophisms (Table S20) (XLSX)

https://doi.org/10.1021/acssynbio.4c00379
ACS Synth. Biol. 2024, 13, 3281−3294

AUTHOR INFORMATION

Corresponding Authors

Arul M. Varman − *Chemical Engineering, School for Engineering of Matter, Transport, and Energy, Arizona State University, Tempe, Arizona 85287, United States;* orcid.org/0000-0003-3028-8941; Email: Arul.M.Varman@asu.edu

Amit Ghosh − *P.K. Sinha Centre for Bioenergy and Renewables, Indian Institute of Technology, Kharagpur, West Bengal 721302, India; School of Energy Science and Engineering, Indian Institute of Technology, Kharagpur, West Bengal 721302, India;* orcid.org/0000-0003-3514-885X; Email: amitghosh@iitkgp.ac.in

Authors

Somdutt Ravindran − *P.K. Sinha Centre for Bioenergy and Renewables, Indian Institute of Technology, Kharagpur, West Bengal 721302, India*

Nima Hajinajaf − *Chemical Engineering, School for Engineering of Matter, Transport, and Energy, Arizona State University, Tempe, Arizona 85287, United States*

Pritam Kundu − *School of Energy Science and Engineering, Indian Institute of Technology, Kharagpur, West Bengal 721302, India*

Jackson Comes − *Chemical Engineering, School for Engineering of Matter, Transport, and Energy, Arizona State University, Tempe, Arizona 85287, United States*

David R. Nielsen − *Chemical Engineering, School for Engineering of Matter, Transport, and Energy, Arizona State University, Tempe, Arizona 85287, United States;* orcid.org/0000-0002-9310-2000

Complete contact information is available at: https://pubs.acs.org/10.1021/acssynbio.4c00379

Author Contributions

[‖]S.R. and N.H.: equal contribution. A.M.V. and A.G.: study conception. S.R.: execution of the model reconstruction and curation. S.R., P.K., and A.G.: execution of the model analysis and interpretations. N.H., S.R., and J.C.: all the experiments. S.R. and N.H.: writing of the original draft. S.R, P.K., D.R.N., A.M.V., and A.G.: performed the review and editing of the whole manuscript. A.M.V. and A.G.: supervision of the whole study. All authors read and approved the final version of the manuscript.

Notes

The authors declare no competing financial interest.

ACKNOWLEDGMENTS

A.G. appreciates the support from the Department of Science and Technology (Grant No. CRG/2020/002080), Department of Biotechnology (Grant No. BT/PR37958/GET/119/297/2020), and Scheme for Promotion of Academic and Research Collaboration (SPARC), MHRD, Government of India (Grant No. SPARC/2019-2020/P1991/SL). This work was also supported in parts by grants from the National Science Foundation (CBET-2146114) to A.M.V. We express our gratitude to Dr. Christopher Jones for generously offering guidance on the utilization of the CO_2 uptake system and extend our appreciation to Sydney Parrish for her invaluable assistance in assembling the CO_2 measurement system.

REFERENCES

(1) Anfelt, J.; Kaczmarzyk, D.; Shabestary, K.; Renberg, B.; Rockberg, J.; Nielsen, J.; Uhlén, M.; Hudson, E. P. Genetic and Nutrient Modulation of Acetyl-CoA Levels in Synechocystis for n-Butanol Production. *Microb. Cell Fact.* **2015**, *14*, No. 167.

(2) Paerl, H. W.; Paul, V. J. Climate Change : Links to Global Expansion of Harmful Cyanobacteria. *Water Res.* **2012**, *46* (5), 1349−1363.

(3) Nozzi, N. E.; Oliver, J. W. K.; Atsumi, S. Cyanobacteria as a Platform for Biofuel Production. *Front. Bioeng. Biotechnol.* **2013**, *1* (September), No. 7.

(4) Vu, T. T.; Hill, E. A.; Kucek, L. A.; Konopka, A. E.; Beliaev, A. S.; Reed, J. L. Computational Evaluation of Synechococcus Sp. PCC 7002 Metabolism for Chemical Production. *Biotechnol. J.* **2013**, *8* (5), 619−630.

(5) Fu, P. Genome-Scale Modeling of Synechocystis Sp. PCC 6803 and Prediction of Pathway Insertion. *J. Chem. Technol. Biotechnol.* **2009**, *84* (4), 473−483.

(6) Iwaki, T.; Haranoh, K.; Inoue, N.; Kojima, K.; Satoh, R.; Nishino, T.; Wada, S.; Ihara, H.; Tsuyama, S.; Kobayashi, H.; Wadano, A. Expression of Foreign Type I Ribulose-1,5-Bisphosphate Carboxylase/ Oxygenase (EC 4.1.1.39) Stimulates Photosynthesis in Cyanobacterium Synechococcus PCC7942 Cells. *Photosynth. Res.* **2006**, *88* (3), 287−297.

(7) Yu, J.; Liberton, M.; Cliften, P. F.; Head, R. D.; Jacobs, J. M.; Smith, R. D.; Koppenaal, D. W.; Brand, J. J.; Pakrasi, H. B. Synechococcus Elongatus UTEX 2973, a Fast Growing Cyanobacterial Chassis for Biosynthesis Using Light and CO2. *Sci. Rep.* **2015**, *5* (1), No. 8132.

(8) Koch, M.; Bruckmoser, J.; Scholl, J.; Hauf, W.; Rieger, B.; Forchhammer, K. Maximizing PHB Content in Synechocystis Sp. PCC 6803 : A New Metabolic Engineering Strategy Based on the Regulator PirC. *Microb. Cell Fact.* **2020**, *19*, No. 231.

(9) Yoshikawa, K.; Toya, Y.; Shimizu, H. Metabolic Engineering of Synechocystis Sp. PCC 6803 for Enhanced Ethanol Production Based on Flux Balance Analysis. *Bioprocess Biosyst. Eng.* **2017**, *40* (5), 791−796.

(10) Włodarczyk, A.; Selão, T. T.; Norling, B.; Nixon, P. J. Newly Discovered Synechococcus Sp. PCC 11901 Is a Robust Cyanobacterial Strain for High Biomass Production. *Commun. Biol.* **2020**, *3* (1), No. 215, DOI: 10.1038/s42003-020-0910-8.

(11) Ng, C. Y.; Farasat, I.; Maranas, C. D.; Salis, H. M. Rational Design of a Synthetic Entner-Doudoroff Pathway for Improved and Controllable NADPH Regeneration. *Metab. Eng.* **2015**, *29*, 86−96.

(12) Deng, M.; Coleman, J. R. Ethanol Synthesis by Genetic Engineering in Cyanobacteria. *Appl. Environ. Microbiol.* **1999**, *65* (2), 523−528.

(13) Atsumi, S.; Higashide, W.; Liao, J. C. Letters Direct Photosynthetic Recycling of Carbon Dioxide to Isobutyraldehyde. *Nat. Biotechnol.* **2009**, *27* (12), 1177−1180.

(14) Lan, E. I.; Liao, J. C. ATP Drives Direct Photosynthetic Production of 1-Butanol in Cyanobacteria. *Proc. Natl. Acad. Sci. U.S.A.* **2012**, *109* (16), 6018−6023, DOI: 10.1073/pnas.1200074109.

(15) Oliver, J. W. K.; Machado, I. M. P.; Yoneda, H.; Atsumi, S. Cyanobacterial Conversion of Carbon Dioxide. *Proc. Natl. Acad. Sci. U.S.A.* **2013**, *110* (4), 1249−1254.

(16) Sawant, K. R.; Sarnaik, A. P.; Savvashe, P.; Hajinajaf, N.; Poole, P.; Varman, A. M.; Lali, A.; Pandit, R. One Cell-Two Wells Bio-Refinery: Demonstrating Cyanobacterial Chassis for Co-Production of Heterologous and Natural Hydrocarbons. *Bioresour. Technol.* **2022**, *363*, 127921.

(17) Lea-Smith, D. J.; Summerfield, T. C.; Ducat, D. C.; Lu, X.; McCormick, A. J.; Purton, S. Exploring the Growing Role of Cyanobacteria in Industrial Biotechnology and Sustainability. *Front. Microbiol.* **2021**, *12*, No. 725128, DOI: 10.3389/fmicb.2021.725128.

(18) Mills, L. A.; Moreno-Cabezuelo, J. Á.; Włodarczyk, A.; Victoria, A. J.; Mejías, R.; Nenninger, A.; Moxon, S.; Bombelli, P.; Selão, T. T.; McCormick, A. J.; Lea-Smith, D. J. Development of a Biotechnology

Platform for the Fast-Growing Cyanobacterium Synechococcus Sp. PCC 11901. *Biomolecules* **2022**, *12* (7), 872.
(19) Qian, X.; Kim, M. K.; Kumaraswamy, G. K.; Agarwal, A.; Lun, D. S.; Dismukes, G. C. Flux Balance Analysis of Photoautotrophic Metabolism: Uncovering New Biological Details of Subsystems Involved in Cyanobacterial Photosynthesis. *Biochim. Biophys. Acta, Bioenerg.* **2017**, *1858* (4), 276−287.
(20) Hendry, J. I.; Prasannan, C. B.; Joshi, A.; Dasgupta, S.; Wangikar, P. P. Metabolic Model of Synechococcus Sp. PCC 7002: Prediction of Flux Distribution and Network Modification for Enhanced Biofuel Production. *Bioresour. Technol.* **2016**, *213*, 190−197.
(21) Broddrick, J. T.; Rubin, B. E.; Welkie, D. G.; Du, N.; Mih, N.; Diamond, S.; Lee, J. J.; Golden, S. S.; Palsson, B. O. Unique Attributes of Cyanobacterial Metabolism Revealed by Improved Genome-Scale Metabolic Modeling and Essential Gene Analysis. *Proc. Natl. Acad. Sci. U.S.A.* **2016**, *113* (51), E8344−E8353.
(22) Ahmad, A.; Pathania, R.; Srivastava, S. Biochemical Characteristics and a Genome-Scale Metabolic Model of an Indian Euryhaline Cyanobacterium with High Polyglucan Content. *Metabolites* **2020**, *10* (5), 177.
(23) Wang, X. Metabolic Engineering of Cyanobacteria for the Biosynthesis of Lipid and Carotenoid. ProQuest Diss. Theses, 2015, No. August, 162.
(24) Hirokawa, Y.; Matsuo, S.; Hamada, H.; Matsuda, F.; Hanai, T. Metabolic Engineering of *Synechococcus elongatus* PCC 7942 for Improvement of 1,3-Propanediol and Glycerol Production Based on in Silico Simulation of Metabolic Flux Distribution. *Microb. Cell Fact.* **2017**, *16* (1), No. 212.
(25) Seaver, S. M. D.; Liu, F.; Zhang, Q.; Jeffryes, J.; Faria, J. P.; Edirisinghe, J. N.; Mundy, M.; Chia, N.; Noor, E.; Beber, M. E.; Best, A. A.; DeJongh, M.; Kimbrel, J. A.; D'haeseleer, P.; McCorkle, S. R.; Bolton, J. R.; Pearson, E.; Canon, S.; Wood-Charlson, E. M.; Cottingham, R. W.; Arkin, A. P.; Henry, C. S. The ModelSEED Biochemistry Database for the Integration of Metabolic Annotations and the Reconstruction, Comparison and Analysis of Metabolic Models for Plants, Fungi and Microbes. *Nucleic Acids Res.* **2021**, *49* (D1), D575−D588.
(26) Kanehisa, M.; Goto, S. KEGG: Kyoto Encyclopedia of Genes and Genomes. *Nucleic Acids Res.* **2000**, *28* (1), 27−30.
(27) Kim, S.; Chen, J.; Cheng, T.; Gindulyte, A.; He, J.; He, S.; Li, Q.; Shoemaker, B. A.; Thiessen, P. A.; Yu, B.; Zaslavsky, L.; Zhang, J.; Bolton, E. E. PubChem in 2021: New Data Content and Improved Web Interfaces. *Nucleic Acids Res.* **2021**, *49* (D1), D1388−D1395.
(28) King, Z. A.; Lu, J.; Dräger, A.; Miller, P.; Federowicz, S.; Lerman, J. A.; Ebrahim, A.; Palsson, B. O.; Lewis, N. E. BiGG Models: A Platform for Integrating, Standardizing and Sharing Genome-Scale Models. *Nucleic Acids Res.* **2016**, *44* (D1), D515−D522.
(29) Saha, R.; Verseput, A. T.; Berla, B. M.; Mueller, T. J.; Pakrasi, H. B.; Maranas, C. D. Reconstruction and Comparison of the Metabolic Potential of Cyanobacteria Cyanothece Sp. ATCC 51142 and Synechocystis Sp. PCC 6803. *PLoS One* **2012**, *7* (10), No. e48285, DOI: 10.1371/journal.pone.0048285.
(30) Suthers, P. F.; Dinh, H. V.; Fatma, Z.; Shen, Y.; Hung, S.; Chan, J.; Rabinowitz, J. D.; Zhao, H.; Maranas, C. D. Genome-Scale Metabolic Reconstruction of the Non-Model Yeast Issatchenkia Orientalis SD108 and Its Application to Organic Acids Production. *Metab. Eng. Commun.* **2020**, *11* (October), No. e00148.
(31) Vu, T. T.; Stolyar, S. M.; Pinchuk, G. E.; Hill, E. A.; Kucek, L. A.; Brown, R. N.; Lipton, M. S.; Osterman, A.; Fredrickson, J. K.; Konopka, A. E.; Beliaev, A. S.; Reed, J. L. Genome-Scale Modeling of Light-Driven Reductant Partitioning and Carbon Fluxes in Diazotrophic Unicellular Cyanobacterium Cyanothece Sp. ATCC 51142. *PLoS Comput. Biol.* **2012**, *8* (4), No. e1002460, DOI: 10.1371/journal.pcbi.1002460.
(32) Yoshikawa, K.; Aikawa, S.; Kojima, Y.; Toya, Y. Construction of a Genome-Scale Metabolic Model of Arthrospira platensis NIES-39 and Metabolic Design for Cyanobacterial Bioproduction. *PLoS One* **2015**, *10* (12), No. e0144430.
(33) Manirafasha, E.; Murwanashyaka, T.; Ndikubwimana, T.; Ahmed, N. R.; Liu, J.; Lu, Y.; Zeng, X.; Ling, X.; Jing, K. Enhancement of Cell Growth and Phycocyanin Production in Arthrospira (Spirulina) Platensis by Metabolic Stress and Nitrate Fed-Batch. *Bioresour. Technol.* **2018**, *255* (November2017), 293−301.
(34) Nzayisenga, J. C.; Sellstedt, A. Metabolomic Study of Heterotrophically Grown Chlorella Sp. Isolated from Wastewater in Northern Sweden. *Molecules* **2021**, *26* (9), No. 2410, DOI: 10.3390/molecules26092410.
(35) Maheswaran, M.; Ziegler, K.; Lockau, W.; Hagemann, M.; Forchhammer, K. PII-Regulated Arginine Synthesis Controls Accumulation of Cyanophycin in *Synechocystis* Sp. Strain PCC 6803. *J. Bacteriol.* **2006**, *188* (7), 2730−2734.
(36) Faizi, M.; Loureiro, C.; Poschmann, G.; Stu, K. Quantitative Insights into the Cyanobacterial Cell Economy. *Elife* **2019**, *8*, No. e42508, DOI: 10.7554/eLife.42508.
(37) Nogales, J.; Gudmundsson, S.; Knight, E. M.; Palsson, B. O.; Thiele, I. Detailing the Optimality of Photosynthesis in Cyanobacteria through Systems Biology Analysis. *Proc. Natl. Acad. Sci. U.S.A.* **2012**, *109* (7), 2678−2683.
(38) Norena-Caro, D. A.; Zuniga, C.; Pete, A. J.; Saemundsson, S. A.; Donaldson, M. R.; Adams, A. J.; Dooley, K. M.; Zengler, K.; Benton, M. G. Analysis of the Cyanobacterial Amino Acid Metabolism with a Precise Genome-Scale Metabolic Reconstruction of Anabaena Sp. UTEX 2576. *Biochem. Eng. J.* **2021**, *171* (December 2020), No. 108008.
(39) Nagy, C.; Haschemi, A. Sedoheptulose Kinase Regulates Cellular Carbohydrate Metabolism by Sedoheptulose 7-Phosphate Supply. *Biochem. Soc. Trans.* **2013**, *41* (2), 674−680.
(40) Steinhauser, D.; Fernie, A. R.; Araújo, W. L. Unusual Cyanobacterial TCA Cycles: Not Broken Just Different. *Trends Plant Sci.* **2012**, *17* (9), 503−509.
(41) Ludwig, M.; Bryant, D. A. Synechococcus Sp. Strain PCC 7002 Transcriptome: Acclimation to Temperature, Salinity, Oxidative Stress, and Mixotrophic Growth Conditions. *Front. Microbiol.* **2012**, *3* (OCT), No. 354.
(42) W, P. P.; Kramer, D. M.; Evans, J. R. The importance of energy balance in improving photosynthetic productivity. *Plant Physiol.* **2011**, *155* (January), 70−78.
(43) Davis, G. A.; Kramer, D. M. Optimization of ATP Synthase c−Rings for Oxygenic Photosynthesis. *Front. Plant Sci.* **2020**, *10* (January), No. 1778.
(44) Van Walraven, H. S.; Strotmann, H.; Schwarz, O.; Rumberg, B. The H+/ATP Coupling Ratio of the ATP Synthase from Thiol-Modulated Chloroplasts and Two Cyanobacterial Strains Is Four. *FEBS Lett.* **1996**, *379*, 309−313.
(45) Muth-Pawlak, D.; Kreula, S.; Gollan, P. J.; Huokko, T.; Allahverdiyeva, Y.; Aro, E. M. Patterning of the Autotrophic, Mixotrophic, and Heterotrophic Proteomes of Oxygen-Evolving Cyanobacterium Synechocystis Sp. PCC 6803. *Front. Microbiol.* **2022**, *13* (May), No. 891895.
(46) Yan, R.; Zhu, D.; Zhang, Z.; Zeng, Q. Carbon Metabolism and Energy Conversion of Synechococcus Sp. PCC 7942 under Mixotrophic Conditions: Comparison with Photoautotrophic Condition. *J. Appl. Phycol.* **2012**, *24*, 657−668.
(47) Liu, X.; Duan, S.; Li, A.; Xu, N. Effects of Organic Carbon Sources on Growth, Photosynthesis, and Respiration of Phaeodactylum tricornutum. *J. Appl. Phycol.* **2009**, *21*, 239−246.
(48) Ebrahim, A.; Lerman, J. A.; Palsson, B. O.; Hyduke, D. R. COBRApy : COnstraints-Based Reconstruction and Analysis for Python. *BMC Syst. Biol.* **2013**, *7*, No. 74, DOI: 10.1186/1752-0509-7-74.
(49) Heirendt, L.; Arreckx, S.; Pfau, T.; Mendoza, S. N.; Richelle, A.; Heinken, A.; Haraldsdóttir, H. S.; Wachowiak, J.; Keating, S. M.; Vlasov, V.; Magnusdóttir, S.; Ng, C. Y.; Preciat, G.; Alise, Ž.; Chan, S. H. J.; Aurich, M. K.; Clancy, C. M.; Modamio, J.; Sauls, J. T.; Noronha, A.; Bordbar, A.; Cousins, B.; El Assal, D. C.; Valcarcel, L. V.; Apaolaza, I.; Ghaderi, S.; Ahookhosh, M.; Ben Guebila, M.; Kostromins, A.; Sompairac, N.; Le, H. M.; Ma, D.; Sun, Y.; Wang, L.;

Yurkovich, J. T.; Oliveira, M. A. P.; Vuong, P. T.; El Assal, L. P.; Kuperstein, I.; Zinovyev, A.; Hinton, H. S.; Bryant, W. A.; Artacho, F. J. A.; Planes, F. J.; Stalidzans, E.; Maass, A.; Vempala, S.; Hucka, M.; Saunders, M. A.; Maranas, C. D.; Lewis, N. E.; Sauter, T.; Palsson, B. Ø.; Thiele, I.; Fleming, R. M. T. Creation and Analysis of Biochemical Constraint-Based Models Using the COBRA Toolbox v. 3.0. *Nat. Protoc.* **2019**, *14* (March), 639−702, DOI: 10.1038/s41596-018-0098-2.

(50) Degtyarenko, K.; De Matos, P.; Ennis, M.; Hastings, J.; Zbinden, M.; Mcnaught, A.; Alcántara, R.; Darsow, M.; Guedj, M.; Ashburner, M. ChEBI: A Database and Ontology for Chemical Entities of Biological Interest. *Nucleic Acids Res.* **2007**, *36* (SUPPL. 1), 344−350.

(51) Caspi, R.; Altman, T.; Billington, R.; Dreher, K.; Foerster, H.; Fulcher, C. A.; Holland, T. A.; Keseler, I. M.; Kothari, A.; Kubo, A.; Krummenacker, M.; Latendresse, M.; Mueller, L. A.; Ong, Q.; Paley, S.; Subhraveti, P.; Weaver, D. S.; Weerasinghe, D.; Zhang, P.; Karp, P. D. The MetaCyc Database of Metabolic Pathways and Enzymes and the BioCyc Collection of Pathway/Genome Databases. *Nucleic Acids Res.* **2014**, *42* (D1), 459−471.

(52) Saltelli, A.; Ratto, M.; Tarantola, S.; Campolongo, F. Sensitivity Analysis for Chemical Models. *Chem. Rev.* **2005**, *105* (7), 2811−2827.

(53) Nobile, M. S.; Coelho, V.; Pescini, D.; Damiani, C. Accelerated Global Sensitivity Analysis of Genome-Wide Constraint-Based Metabolic Models. *BMC Bioinf.* **2021**, *22* (Suppl 2), No. 78.

(54) Sambamoorthy, G.; Raman, K. MinReact: A Systematic Approach for Identifying Minimal Metabolic Networks. *Bioinformatics* **2020**, *36* (May), 4309−4315.

(55) Lercher, M. J.; Oliver, S. G.; Hurst, L. D.; et al. Chance and Necessity in the Evolution of Minimal Metabolic Networks. *Nature* **2006**, *440* (March), 667−670.

(56) Röhl, A.; Bockmayr, A. A Mixed-Integer Linear Programming Approach to the Reduction of Genome-Scale Metabolic Networks. *BMC Bioinf.* **2017**, *18*, No. 2.

(57) Toyoshima, M.; Toya, Y.; Shimizu, H. Flux Balance Analysis of Cyanobacteria Reveals Selective Use of Photosynthetic Electron Transport Components under Different Spectral Light Conditions. *Photosynth. Res.* **2020**, *143* (1), 31−43.

(58) Boyle, N. R.; Morgan, J. A. Flux Balance Analysis of Primary Metabolism in *Chlamydomonas reinhardtii*. *BMC Syst. Biol.* **2009**, *3*, No. 4.

(59) Gudmundsson, S.; Thiele, I. Computationally Efficient Flux Variability Analysis. *BMC Bioinf.* **2010**, *11*, No. 489.

(60) Lakens, D. Calculating and Reporting Effect Sizes to Facilitate Cumulative Science : A Practical Primer for t-Tests and ANOVAs. *Front. Psychol.* **2013**, *4* (November), No. 863.

(61) Kundu, P.; Ghosh, A. Genome-Scale Community Modeling for Deciphering the Inter-Microbial Metabolic Interactions in Fungus-Farming Termite Gut Microbiome. *Comput. Biol. Med.* **2023**, *154* (December 2022), No. 106600.

(62) Mahadevan, R.; Edwards, J. S.; Doyle, F. J. Dynamic Flux Balance Analysis of Diauxic Growth in *Escherichia coli*. *Biophys. J.* **2002**, *83* (September), 1331−1340.

https://doi.org/10.1021/acssynbio.4c00379
ACS Synth. Biol. 2024, 13, 3281−3294